Multi-timescale Parametric Electrical Battery Model for Use in Dynamic Electric Vehicle Simulations

Yue Cao, *Student Member, IEEE*, Ryan C. Kroeze, and Philip T. Krein, *Fellow, IEEE*

***Abstract*— Simulation of electric vehicles (EVs) over driving schedules within a fully dynamic EV simulator requires battery models capable of accurately and quickly predicting state of charge (SOC), *I–V* characteristics, and dynamic behavior of various battery types. An electric battery model utilizing multiple time constants, to address ranges of seconds, minutes, and hours, is developed. The model parameters include open-circuit voltage, series resistance, and equivalent *RC* circuits, with nonlinear dependence on battery SOC. The SOC captures effects from discharge and charge rate, temperature, and battery cycling. Thermal modeling predicting real-time battery temperature is introduced. One focus of this paper is presenting a systematic and generic methodology for parameter extraction as well as obtaining SOC factors through reasonable test work when evaluating any given lithium-ion (Li-ion), nickel-metal hydride, or lead-acid battery cell. In particular, data sets for a Panasonic CGR18650 Li-ion battery cell are tabulated for direct use. The Li-ion battery model is programmed into a MATLAB/Simulink environment and used as a power source within an existing comprehensive dynamic vehicle simulator. Validation of the Simulink model is through a battery testing apparatus with a hardware-in-the-loop driving schedule that cycles real batteries. Results from simulations and measurements of Li-ion battery packs show that the proposed battery model behaves well and interacts appropriately with other subcomponents of the vehicle simulator.**

***Index Terms*— Battery modeling, electric vehicles (EVs), energy storage, lithium-ion (Li-ion) battery, vehicle dynamic simulator.**

I. Introduction

As TRANSPORTATION electrification enters daily life, an accurate dynamic system simulator for electric vehicles (EVs) is a key tool for design and development. Some simulators, such as [1], are based on static maps that reflect steady-state behavior of vehicle subsystems. A dynamic simulator [2]–[3] offers a more detailed look, based on dynamic equations of each subcomponent including the engine, batteries, inverter, motor, transmission, and other parts, down to time scales as fast as microseconds. Often, component models from static simulators and dynamic simulators are not interchangeable because of incompatible time scales. However, a battery model does not require switch-level features as for power electronics. There is the potential for a suitable battery model to capture necessary dynamic details while supporting long-term drive-cycle simulations. This model must accurately represent the terminal voltage, state of charge (SOC), and power losses of several battery types, without excessive simulation times.

In the search for a battery model that supports dynamic analysis sufficient for drive cycle evaluation while avoiding ultrafast details, electrochemical, mathematical, and electrical models of lithium-ion (Li-ion), nickel-metal hydride (NiMH), and lead-acid battery cells have been reviewed. Electrochemical models [4]–[7] are typically computationally challenging owing to a system of coupled time-varying partial differential equations. Such models are best suited for optimization of the physical and material design aspects of internal electrodes and electrolyte [4]. Although battery current and voltage are related to microscopic behavior within each battery cell (e.g., reactant distributions), parameters for electrochemical models are not provided by manufacturers and require extensive investigation [4], [8]. Mathematical models [9], [10] that use stochastic approaches or empirical equations can predict runtime, efficiency, and capacity. However, these models are reported to be inaccurate (5%–20% error) and provide no direct relationship between model parameters and *I–V* characteristics of batteries. As a result, they have limited value in circuit simulation [8].

Electrical models [8], [11]–[17] are intuitive for use in circuit simulations, and can be adapted to comprehensive system-level dynamic models. They often emphasize Thevenin equivalents and impedances. Thevenin models [11]–[13] assume the open-circuit voltage to be constant and use a series resistor and *RC* parallel networks to track battery response to transient loads [8]. An increase in the number of parallel *RC* networks can enhance the accuracy of the predicted dynamic battery response. However, coupling of SOC and time constants with cycle number and temperature leads to relatively high prediction errors for estimating runtime and SOC. Impedance-based models, similar to Thevenin models, are accurate only for a given SOC and temperature set point; hence, their accuracy when predicting dynamic response and battery runtime is limited [14]. Impedance spectroscopy can be used to fit a complicated equivalent network to measured impedance spectra in order to validate time constants to be employed in Thevenin models. Runtime-based electrical models use continuous or discrete-time implementations to simulate battery runtime and dc voltage in SPICE-compatible simulations for constant current discharges. Inaccuracy increases as load currents vary [15]. Combinations of these circuit models, in particular Thevenin and runtime models, can take advantage of the positive attributes of

Manuscript received December 8, 2015; revised March 28, 2016; accepted April 27, 2016. Date of publication May 13, 2016; date of current version December 1, 2016. This work was supported in part by the Grainger Center for Electric Machinery and Electromechanics and in part by the Power Affiliates Program within the University of Illinois at Urbana–Champaign. A preliminary version of this paper was presented at the 2008 IEEE Power Electronics Specialists Conference, Rhodes, Greece [18].

Y. Cao and P. T. Krein are with the Department of Electrical and Computer Engineering, University of Illinois at Urbana–Champaign, Champaign, IL 61801 USA (e-mail: yuecao2@illinois.edu; krein@illinois.edu).

R. C. Kroeze is with Tesla Motors, Palo Alto, CA 94304 USA (e-mail: rkroeze@teslamotors.com).

Digital Object Identifier 10.1109/TTE.2016.2569069

each [8], [16], [17] to achieve accurate SOC prediction, transient response, runtime, and temperature effects. The work presented in this paper seeks such a combination but employs relatively straightforward time-domain tests in place of impedance spectroscopy.

Previous work on MATLAB/Simulink battery models that use electrical approaches [2], [3] was intended for vehicles with lead-acid battery packs. In this paper, a general-purpose three-time-constant dynamic electric battery model, suitable for Li-ion, NiMH, and lead-acid batteries, is developed for use within a dynamic EV simulator. The model is fast enough for drive-cycle-based system-level drivetrain simulation. One focus of this paper is presenting comprehensive time-domain experimental procedures to extract multitime scale parameters for the model. In particular, data sets for a Panasonic CGR18650 Li-ion battery cell are tabulated for direct use. This paper builds on [18] and [19]. The early paper [18] has been cited not only for transportation electrification applications [20]–[23], including review papers [24] and [25], but also for extended fields that include utility applications and stationery energy storage systems [26], [27]. This paper enhances [18] and [19] in the following aspects: 1) refined battery modeling equations for improved accuracy; 2) increased simulation speed by referencing frequency domain; 3) addition of thermal domain modeling to predict real-time battery temperature; 4) detailed model parameter extraction methodology; 5) improved data-fitting equations to eliminate stability limitations; 6) corrected discharge and charge rate factors; 7) addition of temperature factors based on experimental data; 8) inclusion of battery cycle factors; and 9) comprehensive experimental validation of the models and simulator at several levels.

II. Model

A. Prior Work and Initial Model Development

The model in [8] is capable of predicting runtime and I–V performance for portable electronics, but it is not accurate for transient response to short-duration loads (1 s and faster). As a result, it does not accurately predict SOC over a complete drive cycle. Fast time constants of Li-ion batteries have been presented in [13], [16], and [17] and are necessary to determine the losses within a battery pack during vehicle drive cycles. Accurate determination of SOC, which is a function of the discharge or charge rate $i(t)$, temperature $T(t)$, and cycle number n_{cycle} [16], must also include a rate factor $f_1[i(t)]$. The rate factor accounts for a decrease in capacity due to unwanted side reactions [8], [28] as the current increases. This determination of SOC is governed by functions of current, temperature, and cycle count in the form

$$\begin{aligned}\text{SOC}(t) &= \text{SOC}_{\text{initial}} - \int_0^t f_1[i(t)]\cdot f_2[T(t)]\cdot f_3[n_{\text{cycle}}] \\ &\quad \cdot i(t)\cdot\frac{1}{\zeta}dt - \int_0^t i_{\text{self-discharge}}\cdot\frac{1}{\zeta}dt \\ &\approx \text{SOC}_{\text{initial}} - \int_0^t f_1[i(t)]\cdot f_2[T(t)]\cdot f_3[n_{\text{cycle}}] \\ &\quad \cdot i(t)\cdot\frac{1}{\zeta}dt. \end{aligned} \tag{1}$$

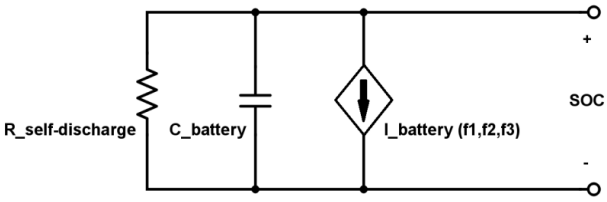

Fig. 1. SOC model based on (1).

In the equation, an initial SOC value should be defined prior to simulation. In this paper, a positive $i(t)$ defines a discharge current, and a negative value represents a charge current. Methods to obtain $f_1[i(t)]$, $f_2[T(t)]$, and $f_3[n_{\text{cycle}}]$ and their relevant data will be discussed in Section III. A separate self-discharge current term is also included; however, it is not an emphasis in this paper, since the model is intended for system simulations over one or a few drive cycles, hence the approximation shown in (1). There must also be a normalization constant ζ, to normalize (1) to battery capacity, representing SOC between 0 and 100%. The factor ζ is defined to be the battery capacity expressed in A · s (equivalent to coulomb but not used here to avoid confusion with the battery capacity rating C). For example, for a 2200-mAh battery cell, the C rating is 2.2 A and $\zeta = 2.2\ \text{Ah} \times 3600\ \text{s/h} = 7920\ \text{A}\cdot\text{s}$. Equation (1) for SOC can be modeled as in Fig. 1. Here I_{battery} is an adjusted battery load ($i(t)\cdot f_1\cdot f_2\cdot f_3$), modeled as a current source, while $R_{\text{self-discharge}}$ is in parallel with the capacitance C_{battery} and represents normalized self-discharge [16].

B. Proposed Model

The proposed model for predicting terminal voltage and power losses of Li-ion, NiMH, and lead-acid batteries is shown in Fig. 2. Built upon Randles' equivalent circuit [29], [30], the model utilizes a multiple-time-constant approach (τ_{sec}, τ_{min}, τ_{hour}) for modeling the transient behavior of the terminal voltage. The transient voltage changes are caused by a battery cell's various internal chemical processes that occur on different time scales. The targets here are in the range of seconds, minutes, and hours [31], [32], consistent with both the needs of EV drive cycle dynamics and experimental results discussed later. Here each parameter is a function of SOC [8], temperature, and battery age [32]. These parameters can be obtained through a series of tests, as will be discussed in Section III. Similar procedures apply if additional time scales are necessary.

The second-, minute-, and hour-based resistors and capacitors predict battery cell dynamics in the corresponding time frames. The designations are somewhat arbitrary (they could be fast, medium, and slow), but typically the actual data are consistent with scales of a few seconds, a few minutes, and several hours. The battery terminal voltage is then calculated as

$$\begin{aligned}V_t = V_{\text{oc}} - i\cdot\Bigg(&R_{\text{series}} + R_{\text{sec}}||\frac{1}{sC_{\text{sec}}} + R_{\text{min}}||\frac{1}{sC_{\text{min}}} \\ &+ R_{\text{hour}}||\frac{1}{sC_{\text{hour}}}\Bigg).\end{aligned} \tag{2}$$

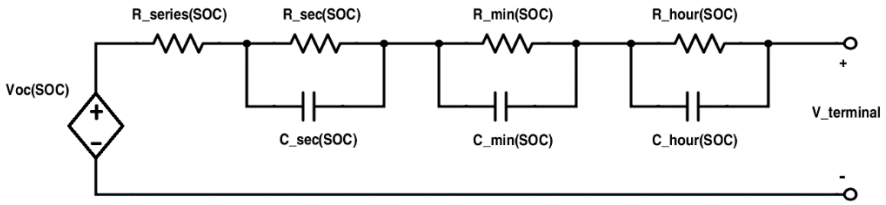

Fig. 2. Three-time-constant approach model for battery terminal voltage and losses.

TABLE I
ONE EXAMPLE SET OF PARAMETERS USED IN (3)

$m\ (kg)$	$A\ (m^2)$	$c\ (J/(kg\cdot°C))$	$T_a\ (°C)$	$h_c\ (W/m^2\cdot°C)$
0.044	4.5×10^{-3}	925	25	10

Note that the equation is presented in Laplace domain with operator s versus time domain as in [18]. Laplace domain representation helps yield fast simulation without requiring solution of exponential and logarithmic equations of RC circuits in time domain.

Calculated $T(t)$ values are required to configure $f_2[T(t)]$, as will be documented in Section III. The temperature changes because of self-heating, and must be solved dynamically so that it couples to the computation of the SOC and subsequently the open-circuit voltage, R, and C parameters from (2). A heat transfer equation utilizing resistive heating and heat exchange [33] is described by

$$mc\frac{dT(t)}{dt} = i^2(t)R_{\text{series}} + \frac{V_{\text{sec}}^2(t)}{R_{\text{sec}}} + \frac{V_{\text{min}}^2(t)}{R_{\text{min}}} + \frac{V_{\text{hour}}^2(t)}{R_{\text{hour}}} - h_cA[T(t) - T_a]. \quad (3)$$

Mass m, external surface area A, and specific heat c are readily measured for a battery cell. Ambient temperature T_a and heat transfer coefficient h_c depend on application details and thermal management designs. A sample set of these values is provided in Table I, from testing of a reference Li-ion battery cell. Equation (3) ignores phase changes, changes in specific heat, and external resistive losses in battery connections. The full vehicle model [2], [3] includes these additional electrical losses.

III. PARAMETER ACQUISITION AND DATA

The circuit model parameters of (1) and (2) are found through a series of experiments using apparatus that consists of data loggers, electronic loads, power supplies, oscilloscopes, and various probes. It is convenient, but not essential, that each instrument can be controlled via LabVIEW, to program test sequences and analyze data. Panasonic CGR18650, 3.7 V, 2200-mAh cylindrical Li-ion batteries are used here as an example to illustrate the parameter acquisition methodologies. This particular battery is popular in available EV applications [34]. Tests are split among multiple packs of battery cells to decrease the effects of cycling during ongoing testing, which includes multiple 100% depth of charging and discharging current profiles. In this paper, 0% SOC is associated with an open-circuit voltage of 3.00 V per cell while 100% SOC is associated with an open-circuit voltage of 4.15 V per cell.

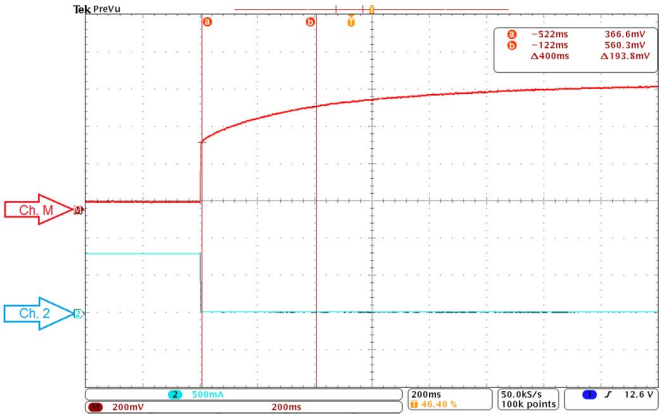

Fig. 3. Terminal voltage (Ch. M) response of discharge current pulse (Ch. 2) test.

A. Determination of Resistor, Capacitor, and Voltage Values at the Three Time Scales

Data for the series resistance R_{series} and resistive and capacitive components of the battery model seconds time constant R_{sec} and C_{sec} are found at various SOC levels via a brief but significant current pulse, recommended to last approximately 1–2 s at C/2. A significant current pulse is chosen such that the voltage response can be easily observed even if only one or a few series connected battery cells are under test. The same current is also suitable for lead-acid batteries; however, a value on the order of 2C would be more appropriate for power-optimized NiMH cells. Figs. 3 and 4 are oscilloscope traces of three series-connected Li-ion cells showing terminal voltage responses at 100% SOC due to discharge and charge current, respectively. Note that Ch. M, which is the terminal voltage less a dc offset value, is zoomed-in view to emphasize fast exponential changes. The immediate voltage jump shown after the current drops to zero in Fig. 3 reflects the discharging series resistance value R_{series}. The exponential voltage rise provides the necessary data for the discharging seconds time constant τ_{sec}, and the steady-state asymptote yields resistance R_{sec}. Capacitance C_{sec} is then found via

$$C_{\text{sec}} = \frac{\tau_{\text{sec}}}{R_{\text{sec}}}. \quad (4)$$

Figs. 3 and 4 correspond to values of $\tau_{\text{sec}} = 0.4$ s and $C_{\text{sec}} = 0.756$ F for discharge and $\tau_{\text{sec}} = 0.328$ s and $C_{\text{sec}} = 0.719$ F for charge, for example. The R_{sec} and C_{sec}

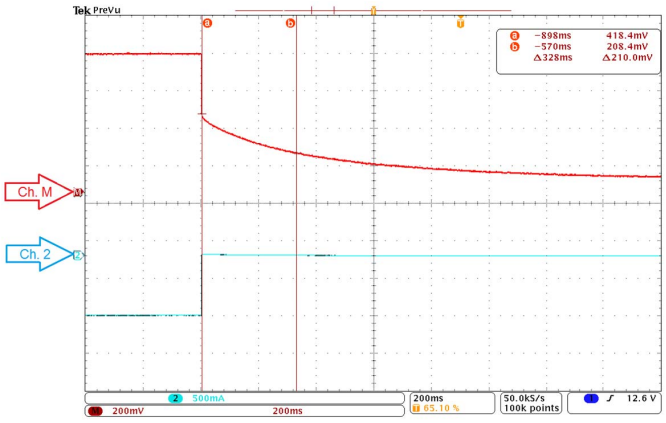

Fig. 4. Terminal voltage (Ch. M) response of charge current pulse (Ch. 2) test.

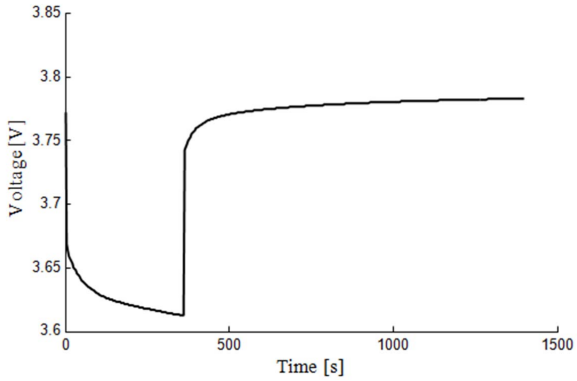

Fig. 5. Terminal voltage response of discharge current test for minutes time constants.

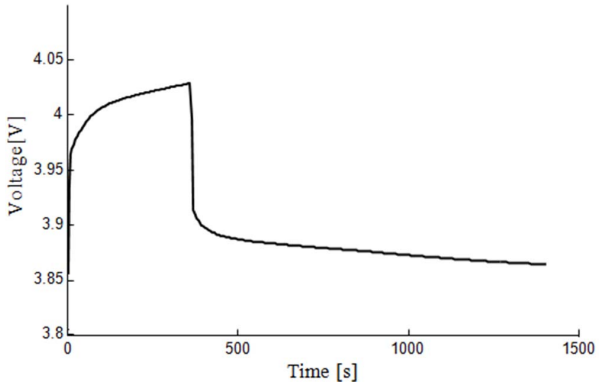

Fig. 6. Terminal voltage response of charge current test for minutes time constants.

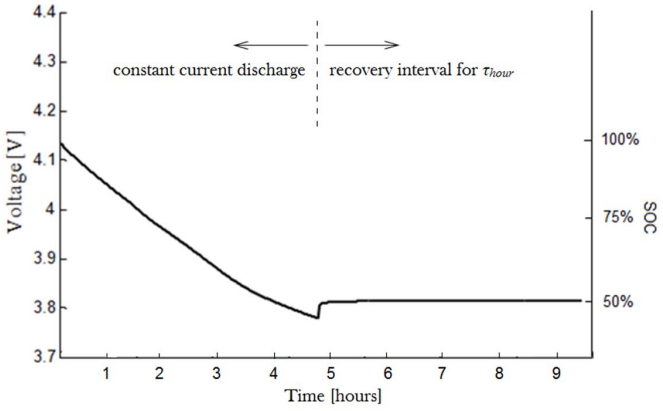

Fig. 7. Terminal voltage response of discharge current test for hours time constants.

values are measured and calculated at 5% intervals across 100%–0% of the battery SOC. Since the discharging current pulse at 100% SOC and the charging current pulse at 0% SOC are short and result in minimal change in SOC, the seconds time-constant circuit parameters can be measured at any SOC level. However, the minutes and hours time constants cannot be obtained at the high and low ends of the SOC spectrum because, for example, it is not possible to measure the minutes time constants by discharging a battery from 105% to 100% SOC or charging a battery from −5% to 0% SOC.

To find the effects of a time constant in the minutes range, an approximate C/2 discharge and charge current profile is imposed on the battery for 6 min, and then the voltage response is recorded for 15 min after the current steps to zero. The test period for the minutes time constant must be long enough to capture the full exponential effect of $\tau_{\min}$ while minimizing battery terminal voltage changes due to τ_{hour}. Figs. 5 and 6 are plots of the measured terminal voltage response at 50% SOC due to the discharging and charging current profiles, respectively. The minutes time constant $\tau_{\min}$ as well as the discharging and charging parameters $R_{\min}$ and $C_{\min}$ can be found from the exponential voltage change and steady-state value. This process is similar to configuration of the seconds parameters described before. Note that both Figs. 5 and 6 include a series-equivalent resistance component, indicated by the immediate voltage jump, which is the sum of previously found R_{series} and R_{sec}. The data in Figs. 5 and 6, for example, correspond to $\tau_{\min} = 63.9$ s and $C_{\min} = 1639.7$ F for discharge and $\tau_{\min} = 89.9$ s and $C_{\min} = 1787.6$ F for charge. The τ_{sec} value is so much faster that no dynamic correction is required.

A constant C/10 charge or discharge current imposed for 5 h, followed by measurement of the battery voltage for 5–10 h after removal of the current, can be used to measure the hours time constant. A small current must be used here so that the voltage response lasts long enough to capture at least three time constants, usually for a few hours, at several SOC values. The values R_{hour} and C_{hour} are measured from initial conditions of 0%, 25%, and 50% SOC for three separate charging tests, and 50%, 75%, and 100% SOC for another three discharging tests. Figs. 7 and 8 show the measured data necessary for calculating the hours time constants at 50% and 100% SOC, respectively, using a current discharge profile from 100% to 50% SOC and a current charge profile from 50% to 100% SOC. In Figs. 7 and 8, the first 5-h records constant current discharging or charging, and the current is turned off afterward for exponential recovery to identify τ_{hour}. Unlike the calculation of seconds or minutes constants, the exponential functions in Figs. 7 and 8 cannot be used directly to calculate R_{hour} and C_{hour} because a correction for $\tau_{\min}$ must

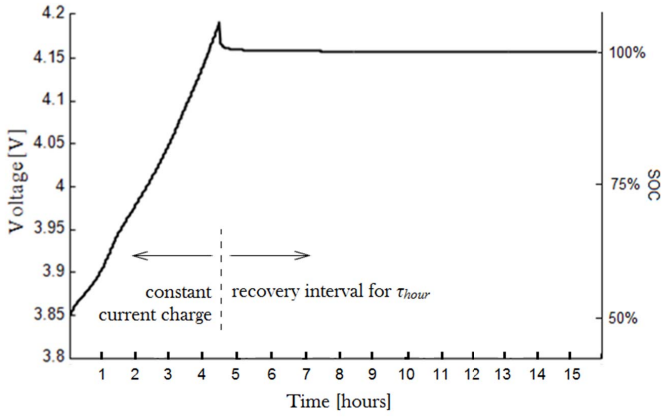

Fig. 8. Terminal voltage response of charge current test for hours time constants.

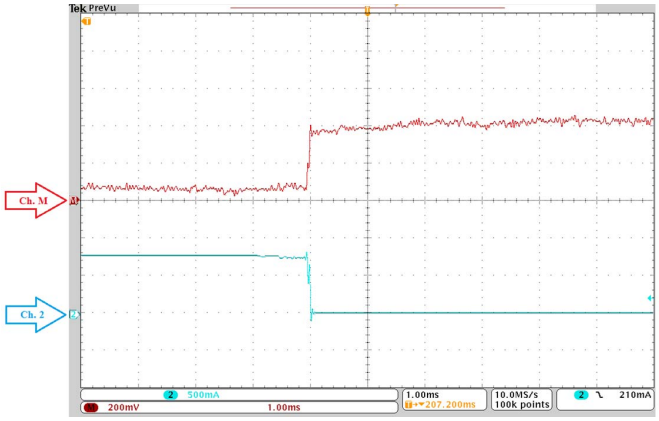

Fig. 9. Zoomed-in view of the terminal voltage (Ch. M) response of discharge current pulse (Ch. 2) at 1 ms scale.

be included according to

$$V_{\text{hour}} = V_{\text{measured}} \pm i(t) \cdot \left[R_{\text{series}} + R_{\text{sec}} + R_{\text{min}}\left(1 - e^{\frac{-t}{\tau_{\text{min}}}}\right)\right]. \tag{5}$$

The remaining V_{hour} is used to extract R_{hour}, C_{hour}, and τ_{hour} similar to the seconds and minutes tests.

In a vehicle, the battery pack interfaces with power components through system power electronics. Time scales faster than τ_{sec} must be checked for any effect on high-frequency switching dynamics. To accomplish this, the region where the battery voltage jumps in Fig. 3 is a zoomed-in view at a scale of 1 ms/div, as shown in Fig. 9. A voltage jump, caused by R_{series} in the battery model, is observed, and it does not show evidence of exponential behavior on this scale. Hence, time scales much faster than τ_{sec} are not beneficial to the purposes of this model.

The open-circuit voltage V_{oc} versus SOC at room temperature is tested and averaged for five Panasonic CGR18650 batteries using a constant current discharge profile. An Agilent data acquisition unit controlled via LabVIEW measures and stores the data for time, current into the battery pack, and terminal voltage of each battery cell during the open-circuit test.

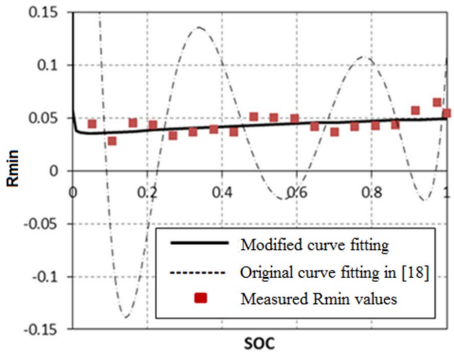

Fig. 10. Modified and original [18] curve fitting for R_{min}.

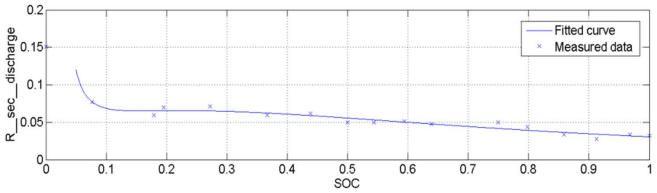

Fig. 11. Modified fitting curve for R_{sec}.

Using a dataset of V_{oc}, R_{series}, R_{sec}, C_{sec}, R_{min}, C_{min}, R_{hour}, and C_{hour} with SOC as the independent variable, model simulations may use either interpolated values between the measured points (i.e., lookup tables) or best-fit mathematical functions. Best-fit functions are not limited to one particular method, and curve-fitting is not a focus of this paper. However, to present the measured data obtained from Panasonic CGR18650 batteries for direct use, this paper modifies a curve-fitting method from [18] in which V, R, and C values were fit into sixth-order polynomial functions of SOC. In the method of [18], some polynomial curves could become negative outside the intended range, which creates instability in a system simulation (Fig. 10). To remedy this here, a logarithmic-polynomial interpolation equation

$$\begin{aligned}\ln(V, R, C) &= a_0 + a_1 \ln(\text{SOC}) + \cdots + a_6 \ln^6(\text{SOC}) \\ &= \sum_{k=0}^{6} a_k \ln^k(\text{SOC})\end{aligned} \tag{6}$$

or

$$V, R, C = \exp\left[\sum_{k=0}^{6} a_k \ln^k(\text{SOC})\right] \tag{7}$$

is employed based on the measured data points. One fitting curve is plotted in Fig. 10 to compare with the original curve from [18]. The new method produces more accurate V, C, and R values and models the battery more robustly. The coefficients of (6) and (7) are listed in Table II. The labels (D) and (C) indicate coefficients for discharging and charging conditions, respectively. Figs. 11 and 12 demonstrate fitting curves for measured R_{sec} and V_{oc} values.

B. Determination of Charge Rate, Discharge Rate, Temperature, and Cycle Factors

Multiple constant current discharge and charge profiles are required to find the discharge and charge rate function $f_1[i(t)]$.

TABLE II
COEFFICIENTS FOR FUNCTIONS USED IN (6) AND FIG. 2

	a0	a1	a2	a3	a4	a5	a6
V_{oc}	1.4222	0.2214	0.1829	0.0745	0.0145	0.0014	5×10^{-5}
R_{series} (D)	-2.9384	-0.2328	-0.2109	-0.1294	-0.0302	0	0
R_{sec} (D)	-3.4883	-1.2434	-0.5619	0.0044	0.0348	0	0
C_{sec} (D)	-0.146	0.3731	1.6511	1.0513	0.1918	0	0
R_{min} (D)	-3.1892	-0.0486	1.4851	6.1491	7.0124	3.1645	0.4997
C_{min} (D)	6.9413	-6.5951	-29.577	-56.356	-46.582	-16.991	-2.2588
R_{hour} (D)	-5.6352	5.1517	12.006	6.1973	0	0	0
C_{hour} (D)	14.622	-6.2451	-19.818	-11.446	0	0	0
R_{series} (C)	-2.8108	0.6011	0.8951	0.436	0.07	0	0
R_{sec} (C)	-3.5637	0.0016	3.4633	4.6412	2.2718	0.425	0.0188
C_{sec} (C)	-0.2737	-3.4945	-14.705	-21.767	-14.113	-4.1803	-0.4632
R_{min} (C)	-2.8744	1.1014	1.1243	0.266	-0.1345	-0.046	0
C_{min} (C)	6.9622	-0.447	2.896	4.5575	2.2427	0.3544	0
R_{hour} (C)	-5.6928	4.3026	10.074	5.1557	0	0	0
C_{hour} (C)	14.666	-5.4723	-18.143	-10.611	0	0	0

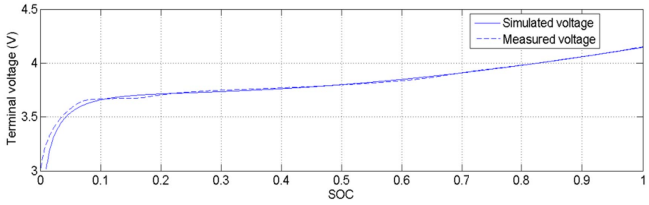

Fig. 12. Modified fitting curve for open-circuit voltage V_{oc}.

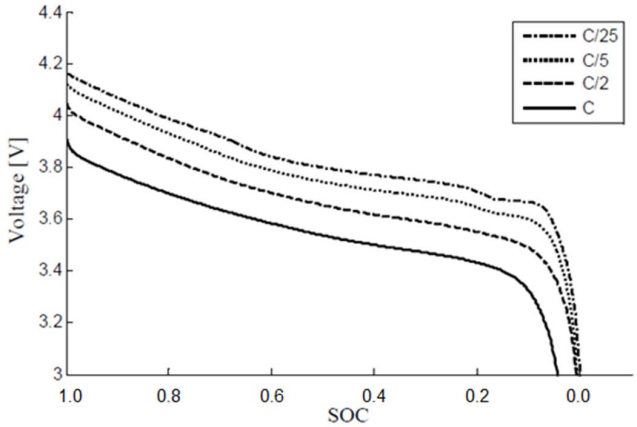

Fig. 13. Terminal voltage under various discharge constant currents.

Fig. 13 plots the measured Panasonic CGR18650 battery terminal voltage as a function of SOC under C/25, C/5, C/2, and C constant discharge currents. The measured discharge voltage in Fig. 13 is defined as V_{measured}. The discharge rate factor

TABLE III
f_1 AND i RELATIONSHIP FOR THE DISCHARGING STATE

i (discharge)	C/25	C/5	C/2	C
$f_1[i(t)]$	1.000	1.005	1.037	1.083

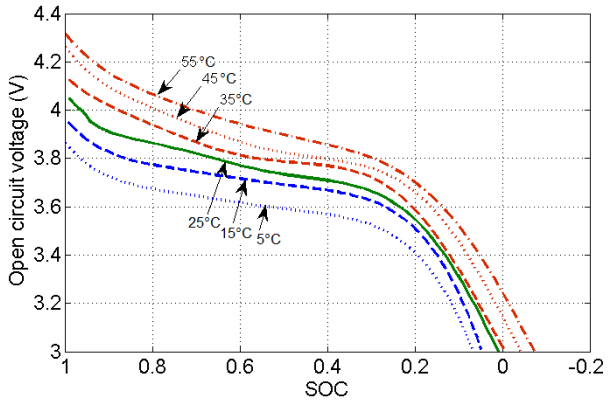

Fig. 14. Open-circuit voltage under various temperatures, based on 0% SOC linked to 25 °C.

requires the computation of a calculated voltage $V_{\text{calculated}}$

$$V_{\text{calculated}} = V_{\text{oc}} \pm i(t) \cdot \left[R_{\text{series}} + R_{\text{sec}}\left(1 - e^{\frac{-t}{\tau_{\text{sec}}}}\right) + R_{\text{min}}\left(1 - e^{\frac{-t}{\tau_{\text{min}}}}\right) + R_{\text{hour}}\left(1 - e^{\frac{-t}{\tau_{\text{hour}}}}\right)\right] \quad (8)$$

so that the discharge rate factor $f_1[i(t)]$ can then be found according to

$$f_1[i(t)] = \frac{\text{SOC}|_{V\_\text{calculated}=3.0\ \text{V}}}{\text{SOC}|_{V\_\text{measured}=3.0\ \text{V}}}. \quad (9)$$

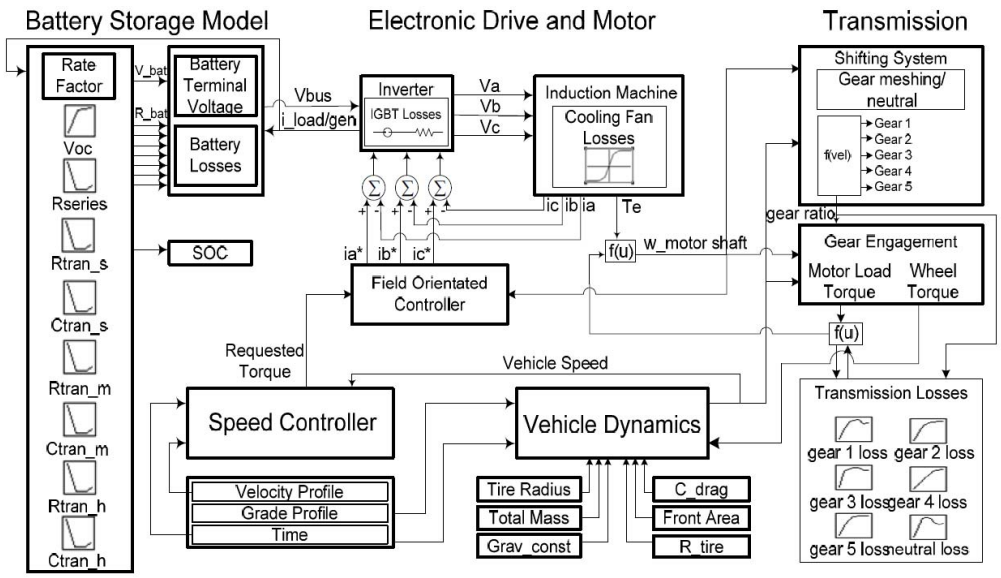

Fig. 15. High-level MATLAB/Simulink block diagram of the HEV simulator [2], [3].

TABLE IV
f_1 AND i RELATIONSHIP FOR THE CHARGING STATE

i (charge)	-C/25	-C/5	-C/2	-C
$f_1[i(t)]$	1.000	1.006	1.019	1.034

That is, the discharge rate factor is the ratio between the SOC when $V_{\text{calculated}}$ crosses the lower voltage threshold (3.0 V) and the SOC when V_{measured} crosses the lower voltage threshold. A low reference discharge current must be selected as a base. In this paper, C/25 is used. Table III presents discharge rate factors for C/25, C/5, C/2, and C. The charge rate factors can be obtained in a similar fashion, as shown in Table IV, except that the ratio is calculated when voltages cross the upper voltage threshold (4.15 V).

Trials of Li-ion battery open-circuit voltage at temperatures of 5 °C–55 °C taken at 10 °C intervals are shown in Fig. 14. Measurement at room temperature, approximately 25 °C, is treated as the reference. This can lead to a negative SOC at low charge and elevated temperature, as shown in Fig. 14. This is not a fundamental problem, since SOC is defined relative to a specific range, but many users may prefer to use a different normalization to maintain positive SOC for all allowed operating conditions. Temperatures above and below room temperature were controlled in an oven or a refrigerator with a maximum ±1 °C error. The temperature factor $f_2[T(t)]$ can be obtained by taking the average of the ratios between each voltage value on the 25 °C curve and the corresponding voltage values on other temperature curves, equivalently described by

$$f_2[T(t)] = \frac{1}{k}\sum_{m=1}^{k}\frac{V_{\text{oc\_}m}|_{25\ ^\circ C}}{V_{\text{oc\_}m}|_{\text{other temperature}}} \tag{10}$$

where k denotes the total number of measured points from each temperature test. Table V displays the

TABLE V
f_2 AND TEMPERATURE RELATIONSHIP

Temperature (°C), $T(t)$	5	15	25	35	45	55
$f_2[T(t)]$	1.0456	1.0169	1.0000	0.9845	0.9675	0.9526

TABLE VI
f_3 AND CYCLE NUMBER RELATIONSHIP

Cycle number, n_{cycle}	0	100	200	300	400	500
$f_3[n_{cycle}]$	1.000	0.953	0.907	0.860	0.846	0.814

calculated $f_2[T(t)]$ results. This open-circuit test is conducted by imposing a discharge current at C/25 with a duty ratio of 50% and a period of one minute. The objective is to avoid battery cell temperature variation due to self-heating.

Battery capacity generally reduces with cycling. For some Li-ion batteries, this relationship is nearly linear and can be found with explicit measurements given in a manufacturer's datasheet [35]. The cycle number is defined as the number of cumulative 100% SOC depletions from a battery cell's initial usage. For example, if a full battery cell is discharged to 60% SOC, recharged to full, and then down to 40% SOC, and back to full again, the combination would count as one cycle. Table VI presents the cycle number factor for the Panasonic CGR18650 battery. The factor is calculated based on the ratio between used battery capacity and new battery capacity indicated on the datasheet. This completes the parameters needed in (1).

IV. MODEL VALIDATION AND RESULTS

Two methods have been utilized to validate the accuracy of the battery model. The first method recreates a standard

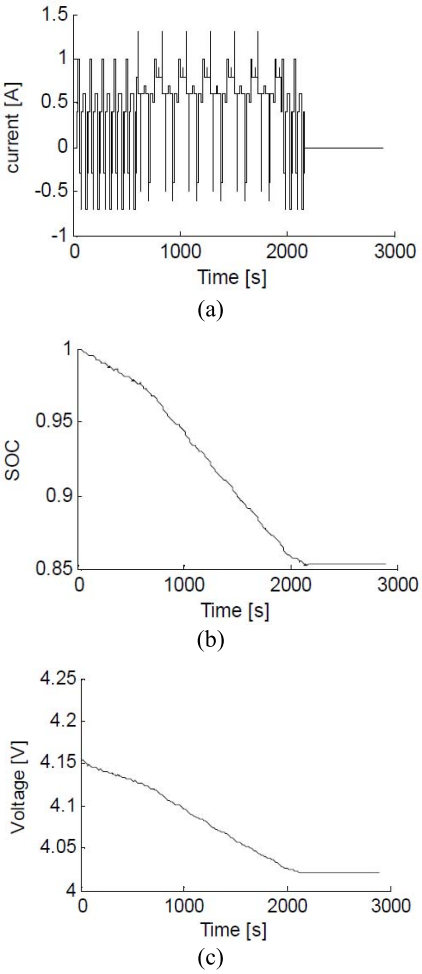

Fig. 16. (a) Current profile. (b) SOC response. (c) Open-circuit voltage response.

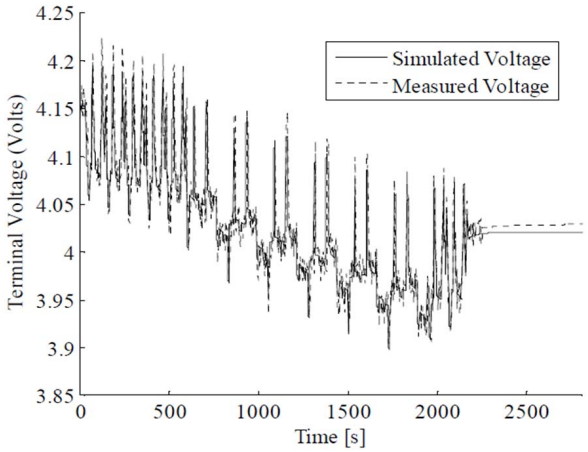

Fig. 17. Simulated and measured terminal voltage responses across the drive cycle.

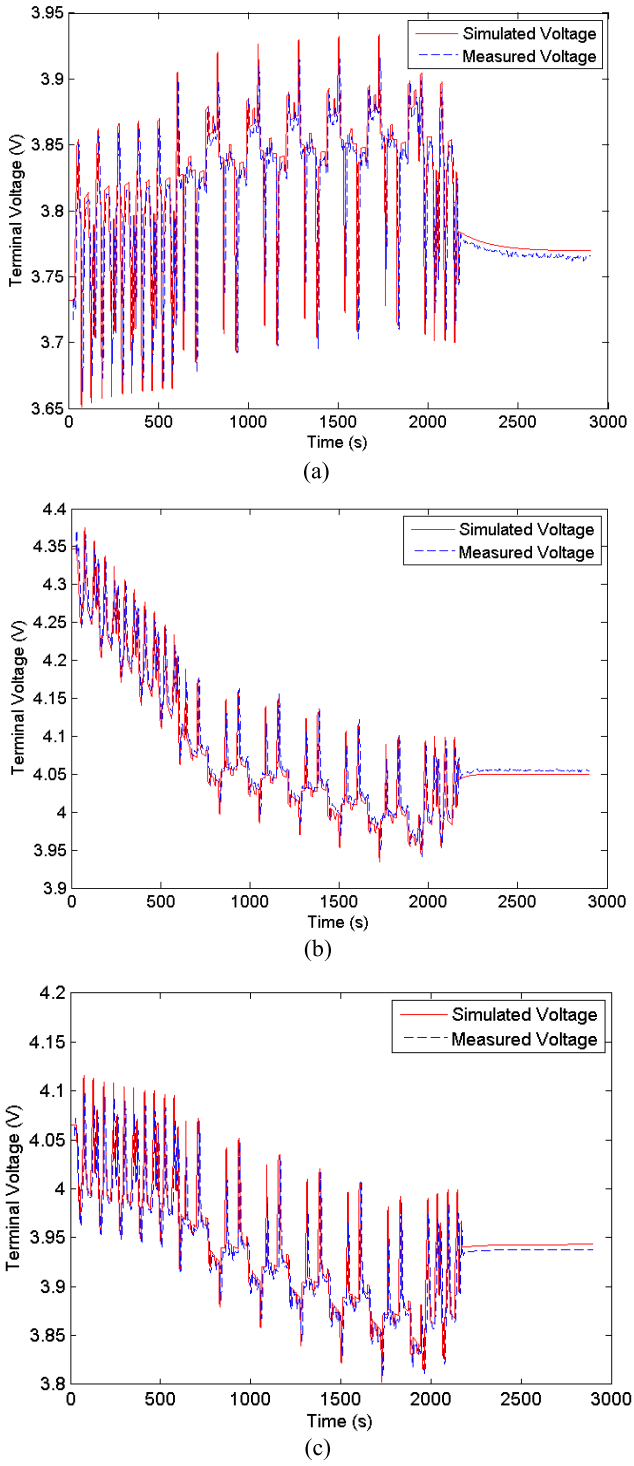

Fig. 18. Simulated and measured terminal voltage responses across the drive cycle for different scenarios. (a) Low initial SOC and reversed current cycle. (b) Ambient temperature at 55 °C. (c) Degraded cell after 200 cycles.

city/highway driving schedule via a current profile, where comparisons between the stand-alone battery simulator and an individual Li-ion battery cell are explored. Hardware-in-the-loop testing for the second method ensures that the battery model behaves correctly within an existing hybrid EV (HEV) simulator [2], [3]. Tests have been performed in MATLAB/Simulink. Fig. 15 depicts the subcomponents of the vehicle simulator, including the battery storage model, as well as the flow of variables between each subcomponent. A detailed discussion of the simulator is provided in [2] and [3].

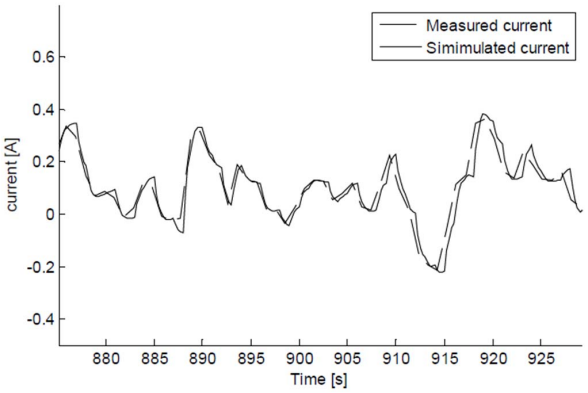

Fig. 19. Simulated and measured battery current responses across FUDS.

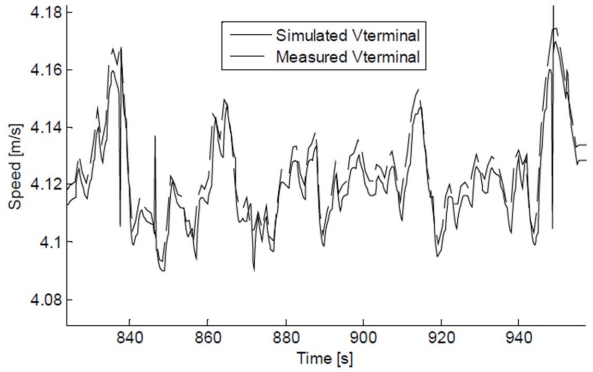

Fig. 20. Simulated and measured terminal voltage responses across FUDS.

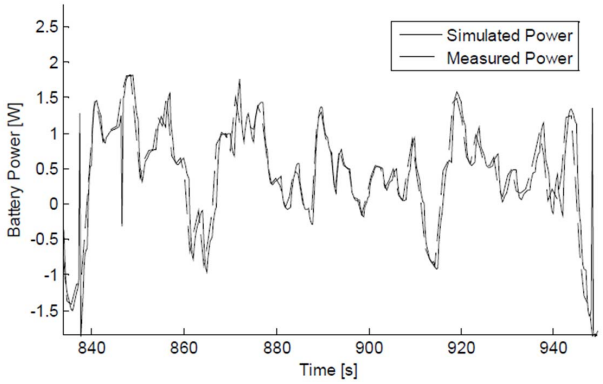

Fig. 21. Simulated and measured battery powers across FUDS.

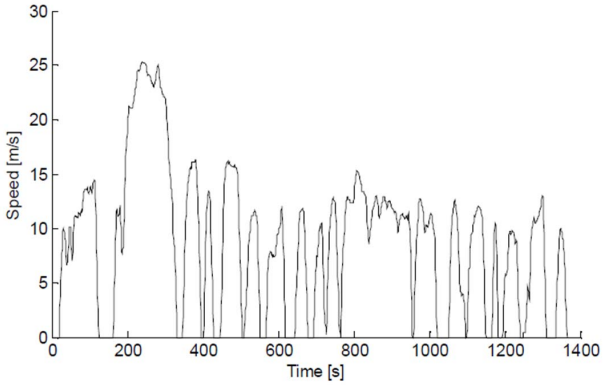

Fig. 22. 22-min FUDS.

Results of verification of the Simulink model against the actual response of tested Li-ion batteries are shown in Figs. 16 and 17. Fig. 16(a) depicts the simulator battery current profile following a city/highway driving schedule. The battery SOC and open-circuit voltage are shown in Fig. 16(b) and (c), respectively. Fig. 17 depicts the simulated battery terminal voltage and measured terminal voltage fluctuations when both the model and batteries are put through the drive cycle. This test utilizes a fully charged new battery cell at room temperature. After this 38-min driving schedule, the error between the actual and simulated terminal voltages is 0.199%. This correlates with SOC deviation not exceeding 1%. Discrepancies between the simulated and measured terminal voltages are found mostly near the peaks and valleys of the voltage during charging periods. This is most likely because the test system sample rate is about 1 Hz, while the simulated driving schedule has faster current charging peaks and valleys. To further validate the model's accuracy and robustness, additional selected simulation and experiments are conducted in the following situations.

1) The battery cell starts at 25% SOC and receives a reversed current profile as in Fig. 16(a).
2) Ambient temperature is held at 55 °C.
3) A degraded battery cell of the same type after approximately 200 cycles is used.

Fig. 18(a)–(c) shows the results of the three scenarios, respectively. Again the error between the measured and simulated terminal voltages is small, not exceeding 1%.

Given the individual cell validation, the Simulink Li-ion battery model, along with the measured model circuit parameters shown previously, is used to simulate a complete battery pack in a drive schedule in the tool described in [3]. The pack uses programmable series and parallel configurations, such as 99S60P here (99 cells in series and 60 in parallel), giving a nominal 366.3 V and 129 Ah. Figs. 19–21 display the simulated and measured individual Li-ion battery's current, terminal voltage, and output power from a window of the 22-min Federal Urban Driving Schedule (FUDS), as shown in Fig. 22, via hardware-in-the-loop tests. The FUDS drive cycle is chosen because it contains wide speed variations and therefore tests the battery model's ability over an extensive range. The proposed battery model successfully represents Li-ion batteries within an EV throughout this driving schedule. Data extracted from the results provide insight into the effects of various driving behaviors and short-term transients on losses within a battery pack. The Simulink model is able to analyze the efficiency of the battery pack during various driving schedules.

V. Conclusion

The proposed multiple-time-constant battery model, using charge and discharge rates, temperature, and cycling factors, accurately represents Li-ion battery cell and pack behavior within a dynamic EV simulator across a complete drive cycle. Methods are presented to extract experimental parameters from basic bench tests. Examples that characterize Panasonic CGR18650 Li-ion cells exemplify methodology to test other Li-ion and NiMH or lead-acid batteries. MATLAB/Simulink models of battery

cell response to simulating driving schedules have been verified using a hardware-in-the-loop dynamic battery testing apparatus. The simulated SOC, terminal voltage, and output power response to city/highway driving schedules tracks the measured responses. The battery model with parameters as discussed supports extensive tests to estimate efficiency and losses within a battery pack during various driving schedules and vehicle dynamic operation strategies.

ACKNOWLEDGMENT

The authors would like to thank J. P. Weinberg for his efforts in obtaining selected experimental data.

REFERENCES

[1] K. B. Wipke, M. R. Cuddy, and S. D. Burch, "ADVISOR 2.1: A user-friendly advanced powertrain simulation using a combined backward/forward approach," *IEEE Trans. Veh. Technol.*, vol. 48, no. 6, pp. 1751–1761, Nov. 1999.

[2] D. L. Logue and P. T. Krein, "Dynamic hybrid electric vehicle simulation, version 1.0," Dept. Elect. Comput. Eng., Univ. Illinois Urbana–Champaign, Champaign, IL, USA, Tech. Rep. UILU-ENG-98-0409, Dec. 1998.

[3] M. Amrhein and P. T. Krein, "Dynamic simulation for analysis of hybrid electric vehicle system and subsystem interactions, including power electronics," *IEEE Trans. Veh. Technol.*, vol. 54, no. 3, pp. 825–836, May 2005.

[4] D. W. Dees, V. S. Battaglia, and A. Bélanger, "Electrochemical modeling of lithium polymer batteries," *J. Power Sources*, vol. 110, no. 2, pp. 310–320, 2002.

[5] L. Song and J. W. Evans, "Electrochemical-thermal model of lithium polymer batteries," *J. Electrochem. Soc.*, vol. 147, no. 6, pp. 2086–2095, 2000.

[6] J. Newman, K. E. Thomas, H. Hafezi, and D. R. Wheeler, "Modeling of lithium-ion batteries," *J. Power Sources*, vols. 119–121, pp. 838–843, Jun. 2003.

[7] P. M. Gomadam, J. W. Weidner, R. A. Dougal, and R. E. White, "Mathematical modeling of lithium-ion and nickel battery systems," *J. Power Sources*, vol. 110, no. 2, pp. 267–284, 2002.

[8] M. Chen and G. A. Rincon-Mora, "Accurate electrical battery model capable of predicting runtime and I-V performance," *IEEE Trans. Energy Convers.*, vol. 21, no. 2, pp. 504–511, Jun. 2006.

[9] P. Rong and M. Pedram, "An analytical model for predicting the remaining battery capacity of lithium-ion batteries," in *Proc. Design, Autom., Test Eur. Conf.*, 2003, pp. 1148–1149.

[10] M. Pedram and Q. Wu, "Design considerations for battery-powered electronics," in *Proc. 36th Design. Autom. Conf.*, 1999, pp. 861–866.

[11] B. Y. Liaw, G. Nagasubramanian, R. G. Jungst, and D. H. Doughty, "Modeling of lithium ion cells—A simple equivalent-circuit model approach," *Solid State Ionics*, vol. 175, nos. 1–4, pp. 835–839, 2004.

[12] C.-J. Zhan *et al.*, "Two electrical models of the lead-acid battery used in a dynamic voltage restorer," *IEE Proc.-Generat., Transmiss., Distrib.*, vol. 150, no. 2, pp. 175–182, Mar. 2003.

[13] B. Schweighofer, K. M. Raab, and G. Brasseur, "Modeling of high power automotive batteries by the use of an automated test system," *IEEE Trans. Instrum. Meas.*, vol. 52, no. 4, pp. 1087–1091, Aug. 2003.

[14] S. Buller, M. Thele, R. W. De Doncker, and E. Karden, "Impedance-based simulation models of supercapacitors and Li-ion batteries for power electronic applications," in *Proc. Conf. Rec. Ind. Appl. Conf. Annu. Meeting*, 2003, pp. 1596–1600.

[15] S. Gold, "A PSPICE macromodel for lithium-ion batteries," in *Proc. 12th Annu. Battery Conf. Appl. Adv.*, 1997, pp. 215–222.

[16] L. Gao, S. Liu, and R. A. Dougal, "Dynamic lithium-ion battery model for system simulation," *IEEE Trans. Compon. Packag. Technol.*, vol. 25, no. 3, pp. 495–505, Sep. 2002.

[17] S. Abu-Sharkh and D. Doerffel, "Rapid test and non-linear model characterisation of solid-state lithium-ion batteries," *J. Power Sources*, vol. 130, pp. 266–274, May 2004.

[18] R. C. Kroeze and P. T. Krein, "Electrical battery model for use in dynamic electric vehicle simulations," in *Proc. IEEE Power Electron. Specialists Conf.*, Jun. 2008, pp. 1336–1342.

[19] R. C. Kroeze and P. T. Krein, "Electrical battery model for use in dynamic electric vehicle simulations," M.S. thesis, Dept Elect. Comput. Eng., Univ. Illinois Urbana–Champaign, Champaign, IL, USA, 2008.

[20] D. Zhao, R. Stobart, G. Dong, and E. Winward, "Real-time energy management for diesel heavy duty hybrid electric vehicles," *IEEE Trans. Control Syst. Technol.*, vol. 23, no. 3, pp. 829–841, May 2015.

[21] Y. Cao and P. T. Krein, "An average modeling approach for mobile refrigeration hybrid power systems with improved battery simulation," in *Proc. IEEE Transp. Electrific. Conf. (ITEC)*, Jun. 2013, pp. 1–6.

[22] Y. Cao, Y. Lei, R. C. N. Pilawa-Podgurski, and P. T. Krein, "Modular switched-capacitor dc-dc converters tied with lithium-ion batteries for use in battery electric vehicles," in *Proc. IEEE Energy Convers. Congr. Expo (ECCE)*, Sep. 2015, pp. 85–91.

[23] C. M. S. Sridharan and P. T. Krein, "Fault modeling and simulation for more-electric aircraft systems," in *Proc. IEEE 16th Workshop Control Modeling Power Electron. (COMPEL)*, Jul. 2015, pp. 1–6.

[24] M. Einhorn, F. V. Conte, C. Kral, and J. Fleig, "Comparison, selection, and parameterization of electrical battery models for automotive applications," *IEEE Trans. Power Electron.*, vol. 28, no. 3, pp. 1429–1437, Mar. 2013.

[25] C. Zhang, K. Li, S. Mcloone, and Z. Yang, "Battery modelling methods for electric vehicles—A review," in *Proc. IEEE Eur. Control Conf. (ECC)*, Jun. 2014, pp. 2673–2678.

[26] M. T. Lawder *et al.*, "Battery energy storage system (BESS) and battery management system (BMS) for grid-scale applications," *Proc. IEEE*, vol. 102, no. 6, pp. 1014–1030, Jun. 2014.

[27] C. Zhao, H. Yin, Z. Yang, and C. Ma, "Equivalent series resistance-based energy loss analysis of a battery semiactive hybrid energy storage system," *IEEE Trans. Energy Convers.*, vol. 30, no. 3, pp. 1081–1091, Sep. 2015.

[28] R. Rao, S. Vrudhula, and D. N. Rakhmatov, "Battery modeling for energy aware system design," *Computer*, vol. 36, no. 12, pp. 77–87, Dec. 2003.

[29] J. E. B. Randles, "Kinetics of rapid electrode reactions," *Discussions Faraday Soc.*, vol. 1, pp. 11–19, Mar. 1947.

[30] A. Lasia *et al.*, "Electrochemical impedance spectroscopy and its applications," in *Modern Aspects of Electrochemistry*, vol. 32, B. E. Conway, J. O'M. Bockris, and R. E. White, Eds. New York, NY, USA: Kluwer, 1999, pp. 143–248.

[31] A. Jossen, "Fundamentals of battery dynamics," *J. Power Sources*, vol. 154, no. 2, pp. 530–538, 2006.

[32] G. Pistoia, *Lithium-Ion Batteries: Advances and Applications*, 1st ed. Atlanta, GA, USA: Elsevier, 2014, pp. 346–360.

[33] A. F. Mills, *Heat Transfer*, 2nd ed. Upper Saddle River, NJ, USA: Prentice-Hall, 1998, pp. 61–105.

[34] *Battery*. accessed Nov. 15, 2015. [Online]. Available: http://my.teslamotors.com/roadster/technology/battery/

[35] *Lithium Ion Batteries: Individual Data Sheet, CGR18650CG Datasheet*, Panasonic, Osaka, Japan, Dec. 2008.

Yue Cao (S'08) received the B.S. (Hons.) degree in electrical engineering with a second major in mathematics from the University of Tennessee, Knoxville, TN, USA, in 2011, and the M.S. degree in electrical engineering from the University of Illinois at Urbana–Champaign (UIUC), Champaign, IL, USA, in 2013, where he is currently pursuing the Ph.D. degree with the Power and Energy Systems Group.

Mr. Cao has been a Power Electronics Engineer Intern with Apple Inc., Cupertino, CA, USA, Halliburton Company, Houston, TX, USA, Flanders Electric, Evansville, IN, USA, and the Oak Ridge National Laboratory, Oak Ridge, TN, USA, in addition to research and teaching. He is currently a Sundaram Seshu Fellow at UIUC, where he was a James M. Henderson Fellow in 2012. His current research interests include power electronics, motor drives, and energy storage with applications in transportation electrification, renewable energy integration, and recently, energy efficient buildings.

Mr. Cao received the Myron Zucker Student Award from the IEEE Industry Applications Society (IAS) in 2010. He has been rated as an Excellent Teaching Assistant for multiple years since 2013. He was the Corresponding Technical Programs Chair of the 2016 IEEE Power and Energy Conference at Illinois. From 2012 to 2013, he served as the President of the IEEE PES/PELS/IAS Student Chapter at UIUC. He served as the Webmaster for the 2009, 2010, and 2012 IEEE Energy Conversion Congress and Exposition. Since 2014, he has been an Invited Reviewer for eight different IEEE TRANSACTIONS or JOURNALS and one IET Journal.

Ryan C. Kroeze received the B.S. and M.S. degrees in electrical engineering from the University of Illinois at Urbana–Champaign (UIUC), Champaign, IL, USA, in 2006 and 2008, respectively.

Mr. Kroeze was an Electrical Engineer and a Senior Staff Architect with the powertrain architecture teams, Tesla Motors, Palo Alto, CA, USA, where he is currently the Manager of motor controls. He holds five U.S. patents.

Mr. Kroeze was a recipient of the Grainger Power Engineering Award from UIUC in 2008.

Philip T. Krein (S'76–M'82–SM'93–F'00) received the B.S. degree in electrical engineering and the B.A. degree in economics and business from Lafayette College, Easton, PA, USA, and the M.S. and Ph.D. degrees in electrical engineering from the University of Illinois at Urbana–Champaign, Champaign, IL, USA.

Dr. Krein was an Engineer with Tektronix, Beaverton, OR, USA, and then returned to the University of Illinois–Champaign. He was a Senior Fulbright Scholar with the University of Surrey, Guildford, U.K., from 1997 to 1998. From 2003 to 2014, he was a Founder and Member of the Board of Directors of SolarBridge Technologies, Inc., Austin, TX, USA, a developer of long-life integrated inverters for solar energy, and now part of Sunpower. He holds the Grainger Endowed Chair Emeritus in Electric Machinery and Electromechanics and is a Professor Emeritus and the Director of the Grainger Center for Electric Machinery and Electromechanics with the University of Illinois–Champaign. He has authored the undergraduate textbook entitled *Elements of Power Electronics—Second Edition* (Oxford University Press, 2015). He holds 34 U.S. patents with additional patents pending. His current research interests include all aspects of power electronics, machines, drives, electric transportation, and electrical energy, with an emphasis on nonlinear control approaches.

Dr. Krein is a Registered Professional Engineer in Illinois and Oregon. He was recognized as a University Scholar in 1999, the highest research award at the University of Illinois–Champaign. In 2003, he received the IEEE William E. Newell Award in Power Electronics. He was the President of the IEEE Power Electronics Society, and served as a member of the IEEE Board of Directors. He is the Editor-at-Large of the IEEE TRANSACTIONS ON POWER ELECTRONICS and an Associate Editor of the IEEE JOURNAL OF EMERGING AND SELECTED TOPICS IN POWER ELECTRONICS. In 2015-2016, he is the Chair of the IEEE Transportation Electrification Community. He was elected to the U.S. National Academy of Engineering in 2016. In 2001, he helped initiate the International Future Energy Challenge, a major student competition involving fuel cell power conversion and energy efficiency.